Global and Planetary Change 189 (2020) 103159

Contents lists available at ScienceDirect

Global and Planetary Change

journal homepage: www.elsevier.com/locate/gloplacha

Research article

Spatial and temporal variability in Mediterranean climate over the last millennium from vermetid isotope records and CMIP5/PMIP3 models

Yael Amitai[a,*], Ruth Yam[a], Paolo Montagna[e], Saverio Devoti[c], Matthias López Correa[b,d], Aldo Shemesh[a]

[a] Weizmann Institute of Science, Rehovot, Israel
[b] Institute of Marine Sciences (ISMAR), National Research Council (CNR), Bologna, Italy.
[c] Institute for Environmental Protection and Research (ISPRA), Rome, Italy.
[d] GeoZentrum Nordbayern, Universität Erlangen-Nürnberg, Erlangen, Germany.
[e] Institute of Polar Sciences (ISP), National Research Council (CNR), Bologna, Italy.

ARTICLE INFO

Keywords:
Mediterranean Sea
Last Millennium
Dendropoma petreaum
Vermetid
CMIP5/PMIP3 models

ABSTRACT

Stable isotope compositions of oxygen ($\delta^{18}O$) and carbon ($\delta^{13}C$) of the aragonite skeleton of the reef-building gastropod *Dendropoma petreaum* provide high-resolution records of the Mediterranean climate over the last millennium. In particular, the isotopic composition of vermetid cores collected from the west and east Mediterranean reveals that the different regions have had distinct thermal and primary production behaviors throughout the last millennium. The rate of warming in the recent Industrial Period is variable among the different regions of the Mediterranean Sea. The $\delta^{18}O$-derived Sea Surface Temperature (SST) anomalies show that the Eastern Mediterranean surface temperature is increasing much more rapidly than in the Western Mediterranean. Additionally, the signals of the Little Ice Age and of the Medieval Climate Anomaly are more apparent in the western and in the central Mediterranean while they are almost absent in the eastern Mediterranean.

We aim to reconcile the SST temporal and spatial pattern with the variability of the North Atlantic Oscillation (NAO) and the South Asian Monsoon (SAM) climate systems by analyzing coupled atmosphere-ocean models from the CMIP5/PMIP3 projects that simulate the global climate of the past 1000 years. We show that even though the NAO is more dominant in the western Mediterranean SST, its latitudinal movement, on a centennial time scale, is evident in the eastern Mediterranean SST signal. We also discuss the Atlantic water inflow role in the observed similarities of the surface productivity signals and the Suess effect that prevail the Industrial Period signal in all regions of the Mediterranean.

1. Introduction

The Mediterranean Sea climate, derived by its location between subtropical and mid-latitude climatic regimes, is characterized by hot and dry summers and wet, cool but mild winters. The North Atlantic Oscillation (NAO) from the northwest and the Asian Monsoon and its derivatives from the southeast are the main global systems that affect the Mediterranean surface water characteristics and influence its temporal and spatial variability. The NAO is the most pronounced pattern of variability in the North Atlantic sea-level pressure, with an anomalous low over Iceland and an anomalous high over the Azores Islands (Hurrell, 1995). This meridional bipolar pattern presents interannual to multidecadal trends in its intensity, position and shape (Jones et al., 1997, 2003; Trouet et al., 2009). A positive (negative) NAO phase is associated with warmer (cooler) conditions over the northwestern part of the Mediterranean Sea and cooler (warmer) conditions over the southeastern part (Hurrell, 1995; Pozo-Vázquez et al., 2001; Trigo et al., 2002; Luterbacher and Xoplaki, 2003). Another global scale climate system influencing the Mediterranean is the South Asian Monsoon (SAM) that remotely affects the eastern Mediterranean through a westward propagating Rossby wave (Rodwell and Hoskins, 1996; Rizou et al., 2018). It implies persistent northerly Etesian winds and strong subsidence over the Eastern Mediterranean (EM), both corresponding with the ascending air over the Bay of Bengal (Tyrlis et al., 2013; Rizou et al., 2018). The EM summer monotonic temperatures are associated with the balance between these two monsoonal effects (Ziv et al.,

* Corresponding author.
E-mail address: yael.amitai@mail.huji.ac.il (Y. Amitai).

https://doi.org/10.1016/j.gloplacha.2020.103159
Received 9 August 2019; Received in revised form 16 December 2019; Accepted 10 March 2020
Available online 12 March 2020
0921-8181/

2004).

The Mediterranean Sea acts as an evaporation basin, water flows in from the Atlantic Ocean at the surface and leaves the Mediterranean at intermediate levels across the Strait of Gibraltar. Surface water, especially in the Western Mediterranean (WM), is strongly affected by the Atlantic Water properties. While this water propagates to the EM, its characteristic changes by becoming warmer, saltier and more oligotrophic. The anti-estuarine circulation evacuates intermediate, nutrient–rich water back to the Atlantic Ocean on a time scale of about 100 years (Roether and Schlitzer, 1991). This type of circulation controls the nutrient concentration, and hence, the primary productivity, which varies from being moderately productive in the WM (Ausín et al., 2015) to an extreme oligotrophic condition in the EM (Berman et al., 1986; Krom et al., 2005, 2014). A mass balance model shows that the bidirectional flows through the Strait of Gibraltar to the WM and through the Strait of Sicily to the EM are the dominant factors controlling the nutrient concentration of the two sub-basins (Powley et al., 2017), with the inflow to the WM being a few times higher in nutrients than the inflow to the EM. However, the presence of other sources of nutrients as riverine or atmospheric deposition can locally modify this general pattern (Herut et al., 1999; Sandroni et al., 2007; Schilman et al., 2001; Jalali et al., 2018).

Over the last millennium climatic changes in the western Mediterranean basin versus those reported in the eastern basin have not always been synchronous (Metaxas et al., 1991; Roberts et al., 2012). The different regions of the Mediterranean Sea respond differently to the external forces influencing them. Satellite observations show opposite trends in Sea Surface Temperature (SST) between the two basins (Macias et al., 2013). The eastern basin is warming at an unprecedented high rate (Luterbacher et al., 2004; Xoplaki et al., 2006; Skliris et al., 2012; Sisma-Ventura et al., 2014), while the western basin exhibits no warming or even a cooling trend, which is associated with the Atlantic Multidecadal Oscillation natural variability (Macias et al., 2013; Vargas-Yáñez et al., 2008). Paleoclimate reconstructions, which are based on marine sediments cores, show centennial SST fluctuations in the Gulf of Lion (Sicre et al., 2016), the Balearic basin (Moreno et al., 2012; Cisneros et al., 2016), Strait of Sicily (Incarbona et al., 2016), and the Aegean sea (Gogou et al., 2016). Some of the observed trends are consistent with our results and a detailed comparison of the regional records is described in the results section.

Changes in productivity were also reported during the last millennium in the WM (Ausín et al., 2015) and the EM (Schilman et al., 2001; Hennekam et al., 2014; Sisma-Ventura et al., 2014). However, the effects described to cause this variability are local, as studied on different time scales. Ausín et al. (2015) proposed that the strength of the Atlantic Jet entering the Alboran Sea governed the WM basin productivity during the Holocene. Schilman et al. (2001) showed a coincidence between Nile floods and EM productivity in the last 1400 years from the analysis of planktonic and benthic foraminifera in sediment cores.

The vermetid *Dendropoma petraeum* is a marine gastropod, adapted to a sessile life style and is abundant around the Mediterranean Sea. The vermetids build reefs composed of dense aggregations of individual aragonite shells, cemented by algae and sets its colonies on rocky shores in the intertidal zone (Safriel, 1975; Calvo et al., 2009). Vermetids precipitate their aragonite skeleton in isotopic equilibrium with the ambient surface seawater (Sisma-Ventura et al., 2014) and serve as archives of high-resolution trends in sea surface properties. Vermetid reefs have been used previously to study climate over the last millennium in the Mediterranean Sea (Antonioli et al., 1999; Silenzi et al., 2004; Montagna et al., 2008; Sisma-Ventura et al., 2009, 2014). Antonioli et al. (1999) established vermetid reefs as indicators for sea-level fluctuations in tectonically stable areas. Silenzi et al. (2004) showed that vermetid reefs capture SST trends and provide paleoclimatic indicators over the last 500 years. Sisma-Ventura et al. (2009, 2014) calibrated $\delta^{18}O$ and $\delta^{13}C$ records from EM vermetid reefs to study climate change at high resolution.

In this paper we use the vermetid based records to suggest a climatic framework for the observed temporal and spatial variability. We compare the skeletal $\delta^{18}O$ and $\delta^{13}C$ composition of fourteen vermetid cores collected from four sampling sites along the Mediterranean Sea and examine the climatic influence on the ambient surface water properties. Earth System Models of the fifth phase of the Coupled Modelling Intercomparison Project (CMIP5) and the third phase of the Paleoclimate Modelling Intercomparison Project (PMIP3) outputs are used to interpret the causes of the observed variations and to separate the externally forced climate signal from the internal variability. The novelty of this study is to compare proxy-based records with outputs from paleoclimate Earth System Models to study the differences between the western and eastern Mediterranean basin. We identify shifts in large-scale climatic systems from west (NAO) and east (SAM) of the Mediterranean Sea by looking at the isotopic differences in the vermetid cores. We suggest that long-term trends in the observed record from the Mediterranean are related to global scale atmospheric patterns and their decadal variability.

2. Material and methods

2.1. Vermetid cores

Fourteen cores of the reef-building gastropod *Dendropoma petreaum* (vermetid) were collected from the Alboran basin (Spain hereafter), the Algerian basin (Tunis hereafter), the Tyrrhenian basin (Sicily hereafter) and the Leventine basin (EM hereafter). They were retrieved using a pneumatic drill from the different basins of the Mediterranean Sea by the late S.Silenzi, G.Sisma-Ventura and Y.Jacobson (Fig. 1; Table 1). Prior to isotope analysis, the cores were cleaned following the method reported in Sisma-Ventura et al. (2009, 2014) and in Jacobson (2018). Each core was continuously sub-sampled at a 3–5 mm interval using a 1 mm diameter dental drill. The purposely coarse sampling diameter removes sub-annual variability and is better suited to examine annual and interannual climate time series. $\delta^{18}O$ and $\delta^{13}C$ analysis was carried out at the stable isotopes laboratory, directed by Prof. Aldo Shemesh in the Department of Earth and Planetary Sciences, at the Weizmann Institute of Science. Dried homogeneous carbonate powders (200–250 μg) from vermetid skeleton were reacted with 100% dry phosphoric acid at 25 °C for 24 h. The samples were analyzed using a Gas Bench II connected inline to Finnigan MAT 252 isotope ratio mass spectrometer. The results are reported in per mil units versus the VPDB standard. The long-term analytical precision of laboratory calibrating material ($\pm 1\sigma$ SD), is 0.06‰ for $\delta^{13}C$ and 0.09‰ for $\delta^{18}O$.

Radiocarbon measurements were made on homogenous vermetid powders at the ANU (Australian National University) radiocarbon dating facility by a Single Stage Accelerator Mass Spectrometer (Fallon et al., 2010); and at the NOSAMS laboratory (National Ocean Sciences AMS Facility, Woods Hole Oceanographic Institution), as detailed in Table S1. Raw radiocarbon dates were converted to calibrated calendar ages by using Calib 7.1 (Stuiver et al., 2017). Reservoir age offset for each core appears in Table S1. An age model was constructed by fitting a line through the collection year (assuming that the reefs were alive at the time of drilling) at the core top as an intercept and through ^{14}C date points. The vermetid cores age-depth relationships of the Eastern Mediterranean are presented in Table1 of Sisma-Ventura et al. (2014) and of the Central and Western Mediterranean in Table S1. The age uncertainty of calibrated ^{14}C generally increases toward the youngest dates. It ranges from 42 to 155 years ($\pm 1\sigma$ SD) with an average uncertainty of 81 $\pm$ 25 year.

The $\delta^{18}O$ and $\delta^{13}C$ composite records from all sites consist of a continuous series with time periods and resolutions as detailed in Tables 1 and S1. Isotopic compositions of vermetids from the Levantine basin were found to be reliable proxies for reconstructing SST and $\delta^{13}C_{DIC}$, based on a multi-years study of living vermetid $\delta^{18}O$ and $\delta^{13}C$

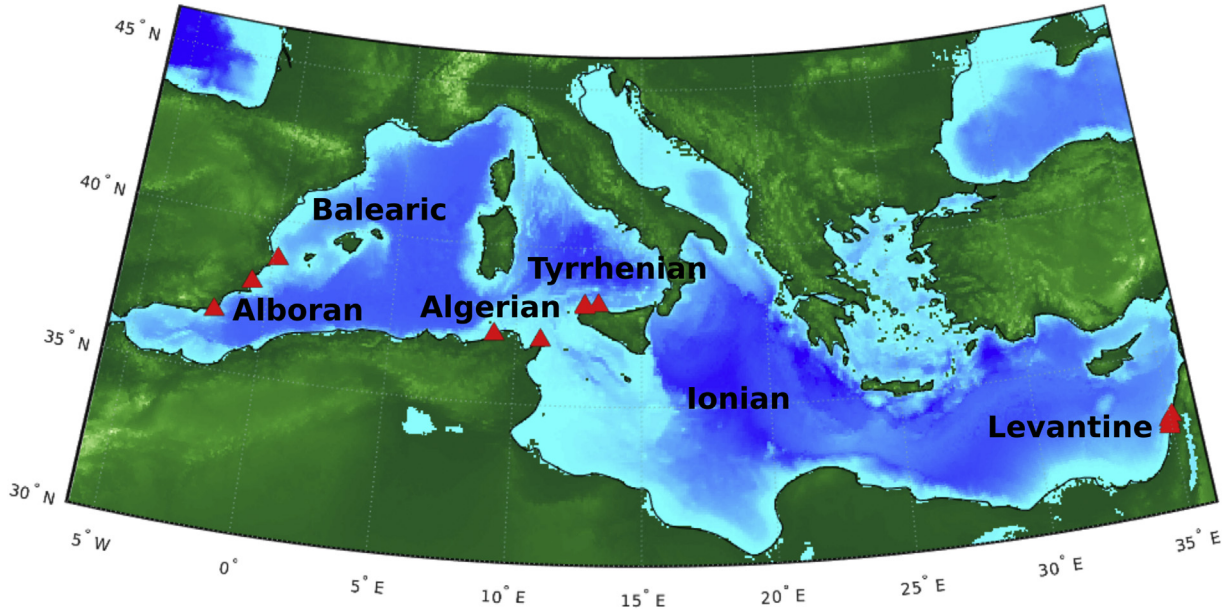

Fig. 1. Map of the Mediterranean Sea showing the sampling locations of the vermetid reefs discussed in the text (red triangles).

Table 1
List of cores and main properties.

Core Location	Core I.D.	Longitude	Latitude	Core Length (cm)	Bot. Age (AD)	Top Age (AD)	Avg Res. (year)
Eastern Mediterranean							
Hazarot Yasaf	HY1	35°04′32.29″E	32°57′51.62″N	17	1090	1282	5.9
Shiqmona	SQ2	34°57′16.00″E	32°49′23.72″N	48.5	1272	1903	8.4
Shiqmona	SQ4	34°57′16.00″E	32°49′23.72″N	21	977	1388	14
Hof Dor	HF3	34°55′25.71″E	32°36′26.42″N	48	1348	1983	6.6
Atlit	AT3	34°56′30.19″E	32°41′20.25″N	36.6	1612	2004	6.6
Tunis							
Sidi Mecrhig	TU1	9°7′58.01″E	37°10′20.06″N	14	488	1978	29
Les Grottes	TU2	10°58′58.13″E	37°3′17.02″N	22	1817	2010	2.8
Sicily							
Cala Mancina	CMA V3	12°42′56.95″E	38°10′33.13″N	23	478	2009	21
Castelluzzo	CAS V1	12°43′25.56″E	38°7′23.55″N	24	1835	1998	9.6
Sferracavallo	SC2	13°15′56.59″E	38°12′1.24″N	13	1696	1997	13.6
Sferracavallo	SC3	13°15′56.59″E	38°12′1.24″N	7	1705	2013	17
Spain							
Javea	JAV	0°11′13.5″E	38°46′52.5″N	13	429	2007	38.9
Punta Prima	PPR	0°42′17.1″W	37°56′28.9″N	10.5	1708	2007	6.9
Cabo De Gata	CDG	2°0′13.30″W	36°51′30.79″	13.5	1807	2008	5.7

variability with respect to the surrounding environment's SST, $\delta^{18}O_{SW}$ and $\delta^{13}C_{DIC}$ (Sisma-Ventura et al., 2009, 2014). Therefore, we extend this to apply to all other studied regions in the Mediterranean. A composite record for the Eastern Mediterranean was constructed by binning data according to the linear age models from five cores (HY1, SQ2, SQ4, HF3 and AT3); for Tunis it was constructed by binning data from two cores (TU1 and TU2); for Sicily from four cores (CMA V3, CAS V1, SC2 and SC3) located at the south Tyrrhenian Sea; and for Spain from three cores (JAV, PPR and CDG) located in the Alboran Sea.

2.2. CMIP5/PMIP3 models

Earth System Models under the CMIP5/PMIP3 project (http://pmip3.lsce.ipsl.fr/) simulate the atmospheric and oceanic system, land use changes (including the terrestrial carbon cycle), and the interactions among these systems. Simulations of past climate with these models provide information about the dynamical processes that lead to hydrological and thermal periods that deviate from millennial averaged climate conditions. The simulations incorporate changes in external forcing parameters (i.e., changes in Earth orbital configuration, volcanic eruptions, solar variations, and anthropogenic changes in the composition of the atmosphere and land use change) following the PMIP3 protocol (Schmidt et al., 2012). We selected the CCSM4 and MPI-ESM-P model outputs of the simulation named *past1000*, started in 850 CE, that was linked to the next *historical* simulation running for the years 1850–2005 CE, for comparison with the millennial vermetid-based records. Both models have the highest spatial horizontal resolution among the CMIP5/PMIP3 models and capture the Industrial Period warming that is well detailed in the global thermal record (Mann and Jones, 2003; Moberg et al., 2005). The CCSM4 model consists of 26 atmospheric vertical levels and a horizontal resolution that corresponds to 80 km longitude × 140 km latitude over the Mediterranean region. It is coupled with an ocean model that has a variable horizontal resolution of about 0.5°, and 60 vertical levels. The MPI-ESM-P model consists of the atmospheric model with horizontal resolution 1.85° that is approximately 160 km longitude × 200 km latitude over the Mediterranean region and 47 vertical levels. The atmospheric model is coupled with the ocean model with a curvilinear grid: 1.5° horizontal resolution

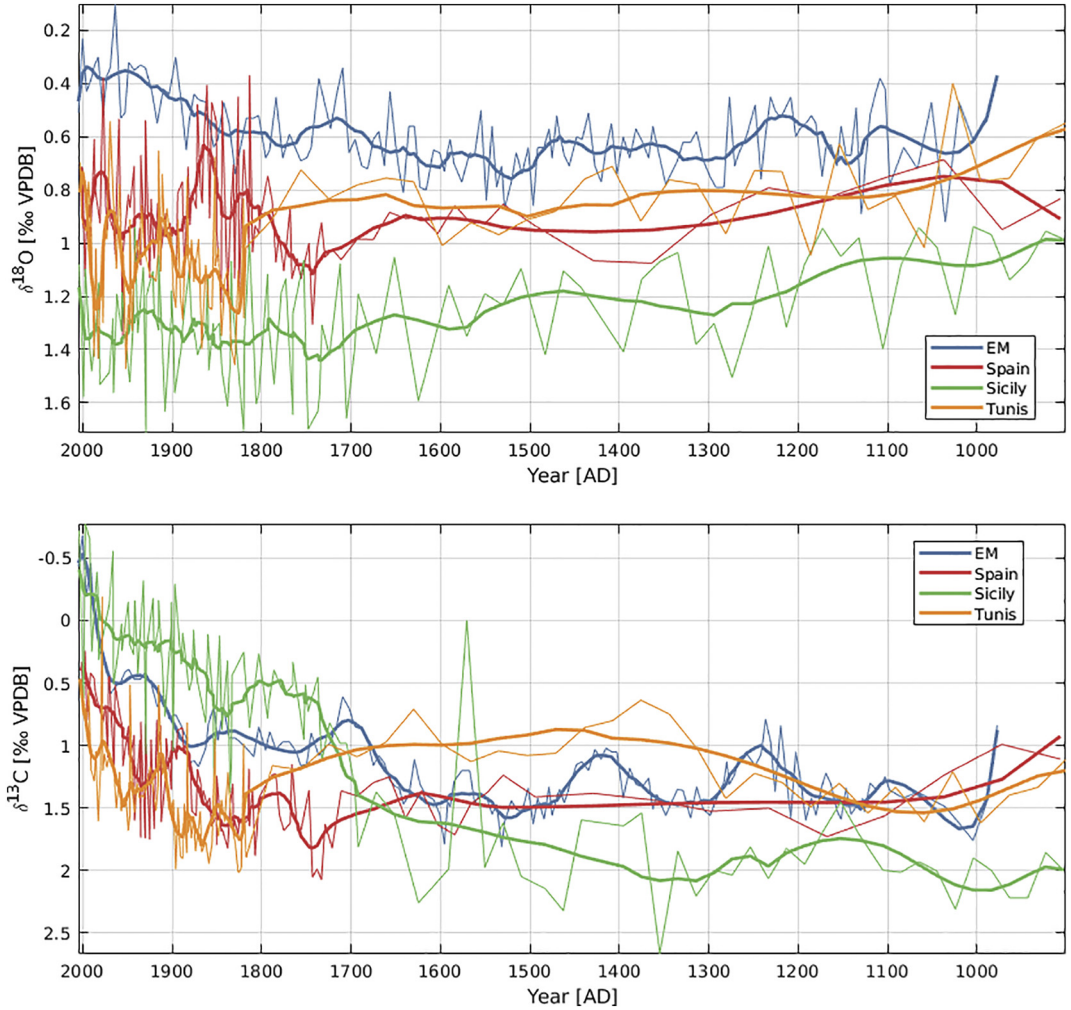

Fig. 2. $\delta^{18}O$ and $\delta^{13}C$ time series over the last ~1000 years from vermetid cores in the locations specified by the triangles in Fig. 1. Unfiltered data in thin lines and Savitzky-Golay filtered data, 7th order polynomial, in thick lines. Note the inverted axes.

with 40 vertical levels. We used monthly averaged atmospheric and oceanic parameters, such as sea level pressure, 500 hPa pressure tendency, ocean temperature, salinity, and horizontal velocity.

Sea level pressures of December, January and February were used to obtain the NAO index time series, according to Hurrell (1995) definition. We calculated Empirical Orthogonal Functions (EOF) of the Atlantic sector surface pressure field from the models, and obtained the first EOF corresponding time series. This was done for each period (Medieval Climate Anomaly and Little Ice Age) separately.

2.3. Data-model comparison

The coupled analysis of proxy-derived paleoclimate records and models has been previously conducted in the Mediterranean (Luterbacher et al., 2012), and it was found that special attention is needed in this comparison exercise. As model output is less relevant at small spatial scales, proxy data usually represent a single site. Therefore, when comparing vermetid-based and model-based time series we focus on identifying long-term trends rather than high-frequency changes that usually result from local (i.e., sub-grid) processes. Additionally, we cope with this characteristic by identifying the underlying large-scale processes, e.g., the NAO and the SAM, that might affect the SST decadal variability captured by the vermetid-based records. We use statistical methods, such as Empirical Orthogonal Functions analysis, which bring the climate modes and shifts into a long-term context, and compare the first mode of variability between significant periods, such as the Little Ice Age and the Medieval Climate Anomaly. This allows subsequent, unbiased comparisons between models (CCSM4 and MPI-ESM-R), simulations, and proxy data that explicitly take into account the estimated errors in the proxy reconstructions and the small-scale resolution issues with models (Lohmann, 2008).

3. Results and discussion

The composite $\delta^{18}O$ and $\delta^{13}C$ records from the four main locations along the Mediterranean Sea (Spain, Tunis, and Sicily in the WM, and Israel in the Levantine basin of the EM) are shown in Fig. 2. The differences between the oxygen isotopic composition records are well evident, with the EM and Sicilian cores showing the lowest and highest $\delta^{18}O$ values, respectively. The $\delta^{18}O$ records from the WM exhibit a trend toward higher values from the beginning of the last millennium until approximately 1700 CE, a trend that is almost absent from the EM record. Another major difference among the four records is observed in the depletion rate of $\delta^{18}O$ during the recent Industrial Period (IP; 1800–2000 CE). The decrease in $\delta^{18}O$ values during the IP is attributed to the climate warming rate, and there is large variance among the different locations. The $\delta^{13}C$ records show higher similarities among the different locations, and the IP $\delta^{13}C$ depletion trend toward lower values, which is associated with the Suess effect (Swart et al., 2010), is well evident in all regions and further demonstrate the reliably of vermetid proxies. Centennial variability characterizes years 1000–1500 CE in the EM $\delta^{13}C$ record but not in the WM; its absence in

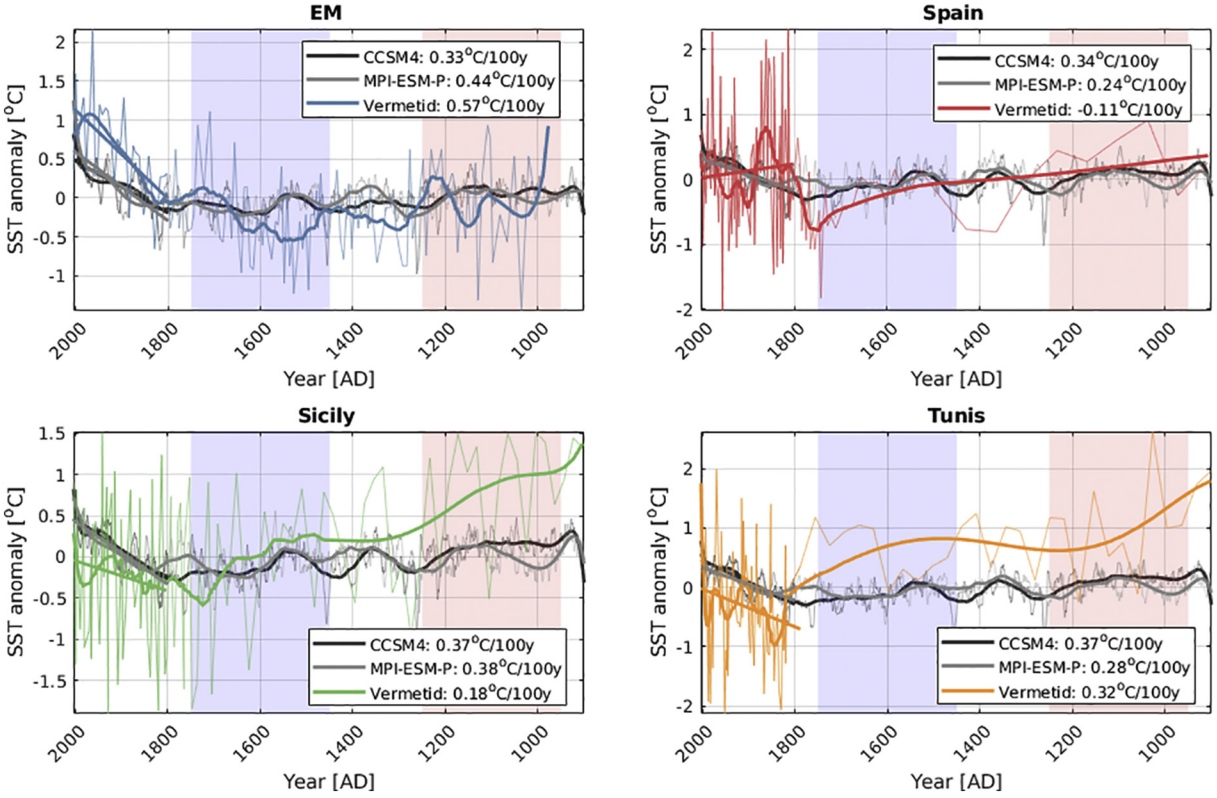

Fig. 3. SST anomalies time series of four CMIP5/PMIP3 models compared with the SST proxy calculated from the vermetid in each location. Shaded areas stand for the Medieval Climate Anomaly (MCA, red 900–1200 CE) and the Little Ice Age (LIA, blue 1400–1700 CE). Slopes in the legend refers to years 1800–2000.

the WM can be due to the lower resolution sampling of the cores across the WM during this period.

3.1. Model simulations compared with vermetids SST anomalies records

The vermetid skeleton's $\delta^{18}O$ is precipitated in equilibrium with the surrounding environment SST and the isotopic composition of the seawater ($\delta^{18}O_{SW}$, Pierre, 1999; Antonioli, 2002). Our records show that the vermetid $\delta^{18}O$ composition follows the surface water temperature gradient from west to east with lighter isotopic values in the EM, corresponding to warmer annual average temperatures, and higher $\delta^{18}O$ values in the WM, corresponding to colder temperatures. For a SST reconstruction, a constant multi-annual $\delta^{18}O_{SW}$ value need to be prescribed, based on stable Atlantic input (Moreno et al., 2012) and Nile flow (Kondrashov et al., 2005). Here, the SST anomalies (and not the SST itself) were calculated from aragonite $\delta^{18}O$ anomalies with a ratio of Δ SST $= -4.4\ \Delta\ \delta^{18}O$ according to the aragonite temperature-dependent fractionation (Böhm et al., 2000). This enable the calculation to be independent from a pre-knowledge of $\delta^{18}O_{SW}$ values. SST anomalies of each region composite were calculated and are presented along with SST anomalies from the models (Fig. 3). Anomalies are calculated from the mean of the entire time span, thus the last millennium.

In this section, we review the main periods (trends) revealed by vermetid-based records and shown by the models to study how the global atmospheric pattern described above has changed over time. We suggest explanations to the observed trends and to the dynamical framework that enables them.

SST anomalies show a warming or slight cooling rate during the IP (1800–2000 CE), which are different among the four locations (as specified by the legend in Fig. 3). The MPI-ESM-P model shows the same trend of IP warming as the vermetids, with the EM that is warming at the fastest rate (0.57 °C/100y and 0.44 °C/100y in vermetid-based and modeled SST records, respectively) and the Spanish trend with the slowest to non-warming rate (−0.11 °C/100y and 0.24 °C/100y in vermetid-based and modeled SST records, respectively). This difference between east and west Mediterranean is also noticed in deep sea sediments cores. While SST cooling trend is observed from cores in the Algerian–Balearic basin over the IP (Moreno et al., 2012; Cisneros et al., 2016), an unprecedented warming rate is evident from cores in the Aegean basin (Gogou et al., 2016) over the same period. However, a SST reconstruction from the Gulf of Lion shows a significant SST warming trend over the IP (Sicre et al., 2016) that is not evident in our records. A short, but distinct warm period is observed in 1850 CE from foraminifera record from both the Balearic basin (Margaritelli et al., 2018) and the Tyrrhenian basin (Margaritelli et al., 2016). However, we identify this SST positive anomaly in 1850 CE only in our Spanish record and not in the Sicilian one (Fig. 3). Sediment cores in the Strait of Sicily do not show distinct trend in SST over the IP (Incarbona et al., 2016), similarly to our vermetid-based record.

The shaded areas in Fig. 3 stand for the Medieval Climate Anomaly (MCA, red 900–1200 CE) and the Little Ice Age (LIA, blue 1400–1700 CE) according to Mann et al. (2009). The long-term cooling trend between the MCA and the LIA is observed in the Spanish, Sicilian, and Tunisian vermetid-based SST anomaly records, as well as in the models time series, although less distinctly. The EMs vermetid-based record also shows a shift between the MCA to LIA but to a much lesser extent. Overall, the SST anomalies from the models match quite well the range of SST anomalies from the proxies, taking into account that the models grid cell covers a large area (50–100 km resolution) and does not represent local effects.

Other proxy-based records also show an overall cooling of SST between the MCA and the LIA in the WM (see Moreno et al., 2012; Cisneros et al., 2016, e.g., in the Algeriane–Balearic cores), with high frequency fluctuations that are not resolved in our records. We do

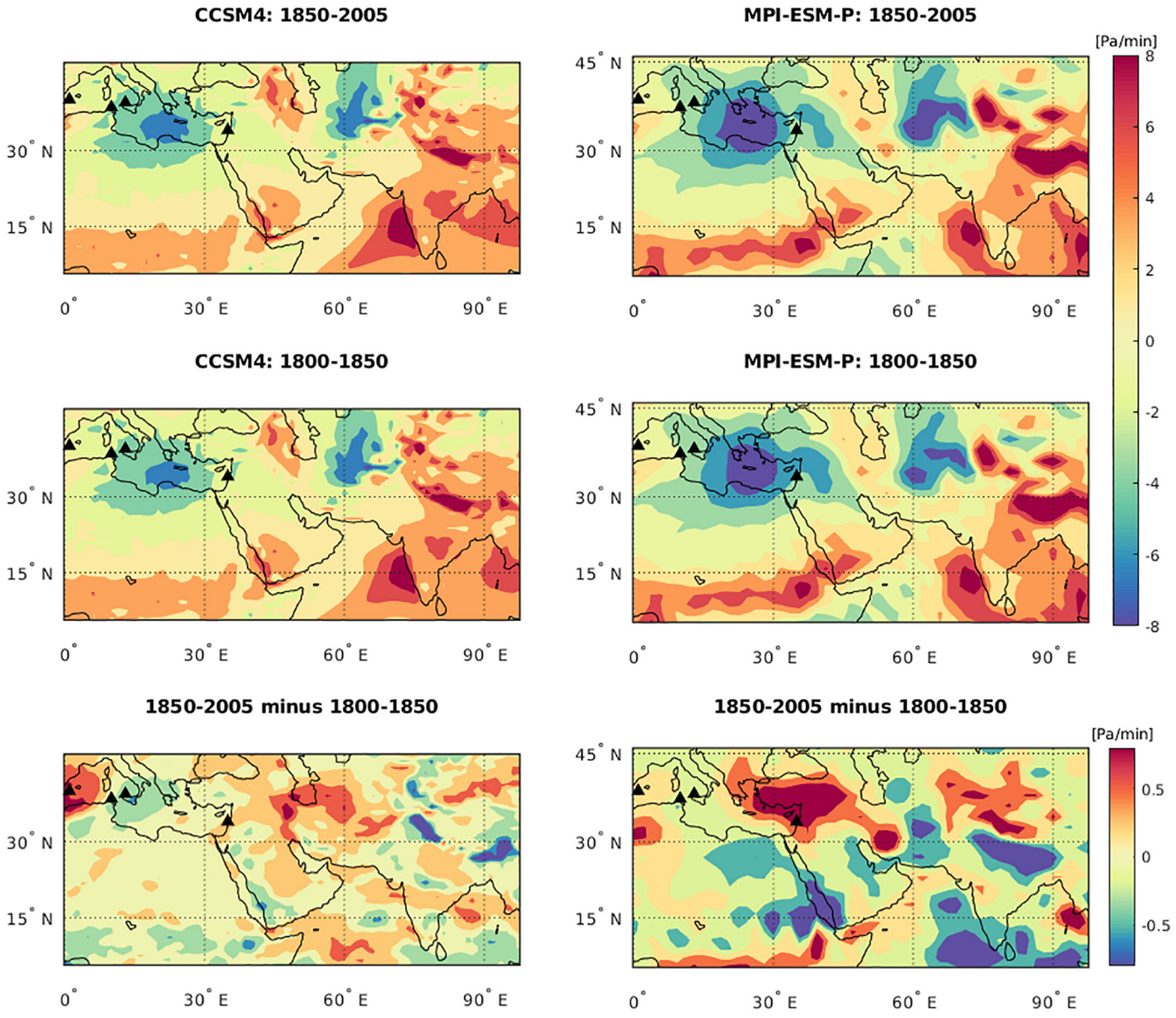

Fig. 4. Pressure tendency from the CMIP5/PMIP3 models in July at 500 hPa over the South Asian Monsoon and the Eastern Mediterranean area in the Industrial Period (1850–2005), the Pre-Industrial Period (1800–1850) and the difference between them. In the two upper rows, blue (red) colors denote subsidence (ascent).

observe a cold period around 1750 CE in our Spanish and Sicilian records, that correspond to the reported Maunder cold event recorded by planktonic foraminiferal in the Balearic basin (Cisneros et al., 2016; Margaritelli et al., 2018) and in the Tyrrhenian basin (Margaritelli et al., 2016). The Maunder cold temperature anomaly in these foraminifera records is not manifested in our modeled SST anomalies record (Fig. 3) and is associated with Atlantic Blocking event (Margaritelli et al., 2016, 2018). Furthermore, the Aegean sediment record shows distinct warm anomaly at about 1600 CE followed by rapid cooling until 1700 CE (Gogou et al., 2016) that we do not capture in our vermetid records.

In order to understand the enhanced IP warming rate of the EM, we obtained maps of the 500 hPa pressure tendency in July of the South Asian Monsoon and the EM regions during the IP (1st row of Fig. 4), prior to the IP (2nd row of Fig. 4), and the difference between those periods (3rd of Fig. 4). The maps of the 500 hPa pressure tendencies are used to first identify the subsidence over the EM region during summer, as it is the prominent descending branch of the ascending air due to the Monsoon circulation over South Asia (Rodwell and Hoskins, 1996; Tyrlis et al., 2013), and is seen in minimal values in both models. Second, the difference in the strength of the subsidence is examined, as it is directly related to the strength of the Monsoon (Tyrlis et al., 2013; Rizou et al., 2018; Katrantsiotis et al., 2019). When subtracting the Pre-IP map from the IP map, a positive anomaly over the EM is obtained by the MPI-ESM-P model, and a positive anomaly over Iran (where the secondary descending branch is located) is obtained by the CCSM4 model. Both indicate that the SAM effect over the EM has weakened during the IP. We note that the MPI-ESM-P model shows an enhanced EM warming (in good agreement with the vermetid-based IP trends) while exhibiting a weaker monsoonal effect over the exact same region, i.e., the EM. This implies that the MPI-ESM-P model represents well the IP atmospheric dynamics over the EM. This Monsoon weakening trend was also suggested on the basis of decrease in precipitation over the last five decades in India (Krishnan et al., 2016, and references within) and significant reduction in surface south-westerly winds over South Asia (Rao et al., 2004; Sathiyamoorthy, 2005; Abish et al., 2013). The counteract effect of EM warming by large-scale subsidence is the EM cooling by northerly Etasian winds, both driven by the SAM and prevail

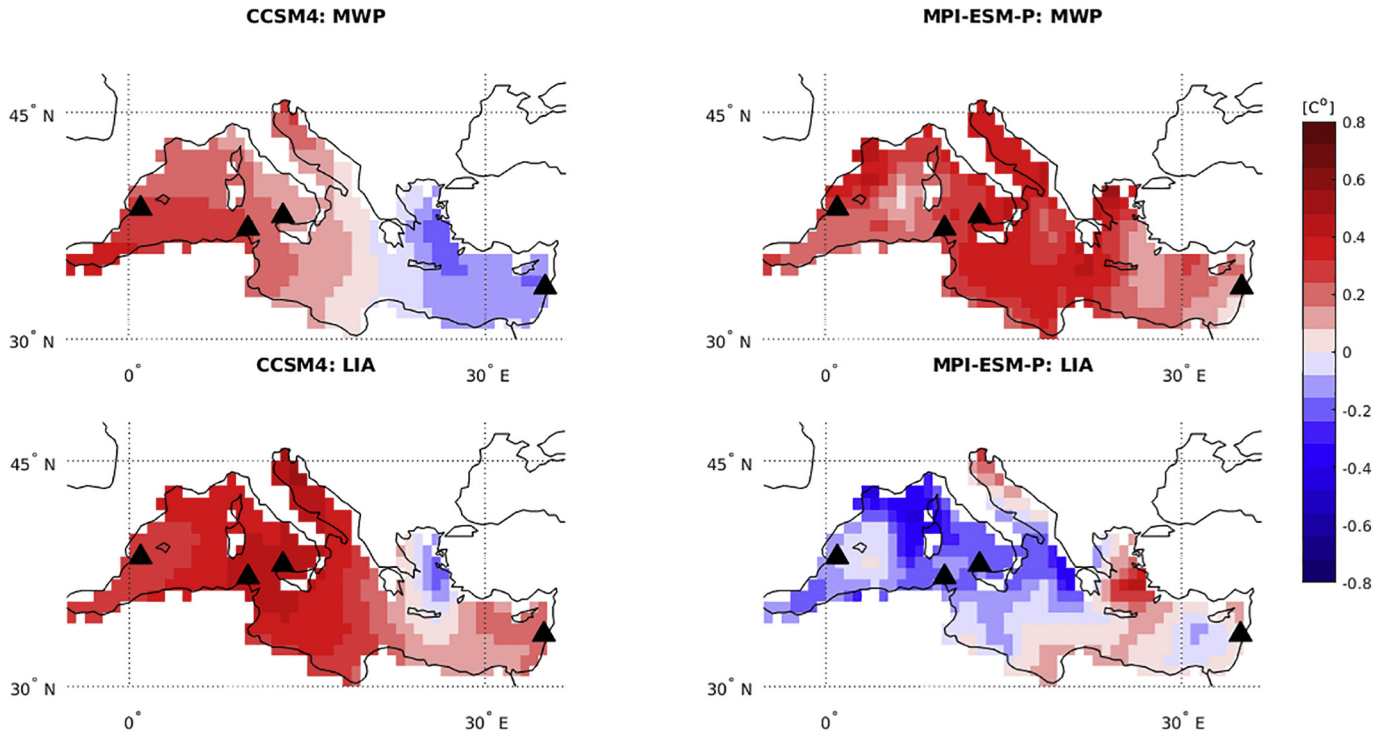

Fig. 5. Mediterranean SST difference from the CMIP5/PMIP3 models between years with positive NAO index minus negative NAO index during MCA (900–1200 CE; upper row) and during LIA (1400–1700 CE; lower row). Vermetid rough locations are in black triangles.

the EM summer air temperature. The decrease in the strength of the cooling Etasian winds is more effective than the large-scale subsidence (Poupkou et al., 2011; Tyrlis et al., 2013; Harpaz et al., 2014; Katrantsiotis et al., 2019) and might explain the high warming rate that the EM experiences when the Asian Monsoon is weakening. While our analysis shows a good agreement between the modeled impact of the SAM on the EM SST and the vermetid-based record high warming rate, Anderson et al. (2002) suggest a different scenario. They suggest enhanced Arabian Sea upwelling, which is the result of an intensification of the monsoon winds during the IP.

We next examine the MCA/LIA transition, which is characterized by a cooling trend in the SST anomaly time series of both vermetid and models (Fig. 3). The periods 900–1200 and 1400–1700 represent broadly the MCA and the LIA, respectively. Note that we chose a broad temporal range to define the MCA and LIA on account that global SST records show that those periods are not necessarily synchronized in time over different oceanic regions (Saenger et al., 2011). Since the North Atlantic regime is a major source of variability to the Mediterranean basin (Josey et al., 2011; Marullo et al., 2011; Moreno et al., 2012; Roberts et al., 2012; Grauel et al., 2013; Goudeau et al., 2015; Ausín et al., 2015; Bonomo et al., 2016; Cisneros et al., 2016; Margaritelli et al., 2016), its first mode of variability the North Atlantic Oscillation is being examined in relation to the modeled Mediterranean's summer SST maps. We calculated an EOF-based NAO index from the same models that simulated the Mediterranean's summer SST anomalies, considering a dynamical connection between the North Atlantic and the Mediterranean regions.

We choose the 30 years with the highest NAO index (out of 300 years of MCA and LIA) and averaged the Mediterranean summer SST of those years. The same was done with the 30 years with the lowest NAO index. The summer's SST difference between highest NAO index years and lowest NAO index years is presented in Fig. 5 for both models and both periods, MCA (upper row) and LIA (lower row). The CCSM4 model suggests that during the MCA the EM responded opposite from the WM to the NAO. The EM cooled and the WM warmed under positive NAO index years, as observed for present day (Hurrell, 1995). However, during the LIA, the WM and EM responded similarly, being warmer under positive NAO index years. The results are not as clear in the MPI-ESM-P model, where the entire Mediterranean Sea is warmer under positive NAO index years during the MCA and most of it is cooler under positive NAO index years during the LIA. However, the different response of the Mediterranean's summer SST to NAO phases between the two periods is well evident in the MPI-ESM-P model as well. Furthermore, both models show that the WM SST difference between opposite NAO phases is higher than in the EM for both periods (See Fig. 5).

To understand the dissimilarity between the MCA and the LIA, we study the source of variability, the North Atlantic surface pressure anomalies. We obtained the NAO pattern in surface pressure anomalies units by regressing surface pressure anomalies on the first EOF principle component. This was done for each period separately and is presented together with the difference between patterns in Fig. 6. Both models exhibit a positive anomaly in the center of the North Atlantic, suggesting that during the MCA the centers of anomalous pressure were more northern than they were during the LIA. This suggests that in the LIA, the subtropical jet, which is associated with the NAO pattern, was located further south than it was in the MCA and that the EM reaction to the NAO phase was as the WM (warmer under positive NAO phase). We note that in the MPI-ESM-P model the positive pressure anomaly is more shifted to the north, implying that the large difference in the Mediterranean's SST maps between the two periods (Fig. 5, right column) results from the extreme latitudinal shift of the NAO centers. During the MCA, the MPI-ESM-P model shows that the entire Mediterranean SST is reacting as the WM reacts to NAO at the present day, hence warmer under positive NAO phase. This suggests that the MPI-ESM-P model describes an unusual southern NAO pattern and that the CCSM4 model might better represent the dynamics of the North Atlantic sector. Another possible reason for the MPI-ESM-P unusual result is that during the LIA, when the NAO seems to shift south in both models, the WM could have experienced Greenland-like conditions (SST colder under positive NAO phase; Fig. 5). A low-frequency, centennial variability in the NAO phase was previously described by Saenger et al.

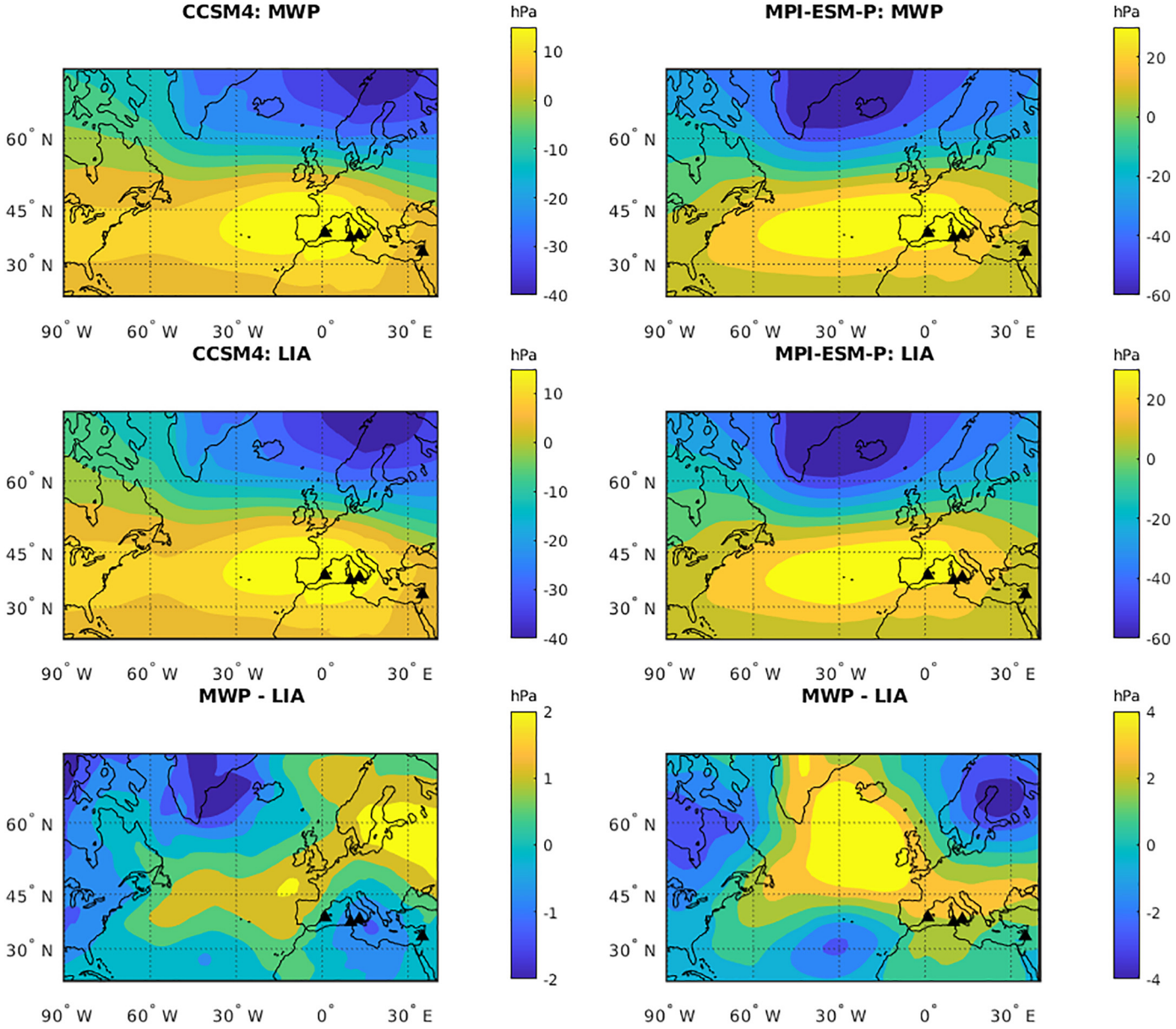

Fig. 6. North Atlantic Oscillation pattern calculated from the first EOF of the sea level pressure anomalies from the CMIP5/PMIP3 models during the MCA (900–1200 CE), the LIA (1400–1700 CE) and the difference between them. The values are presented in hPa and obtained by regressing the sea surface pressure anomalies over the first principal component time series.

(2011). They have attributed this variability to irradiance variations, stating that strong irradiance during 700–1250 CE (around our definition of MCA) resulted in a more positive NAO phase and reduced irradiance after 1250 CE in a more negative phase of the NAO. A shift in the NAO centers accompanied by an increased storm track activity was also reported by Ulbrich and Christoph (1999) under IP climate change.

We further examine the Mediterranean's summer SST response to the SAM system, to ensure that the MCA/LIA cooling signal observed is not derived from a tropical source of variability. We used a SAM index that is related to the Mediterranean sector (Tyrlis et al., 2013) by averaging the 500 hPa pressure tendency over a box (17–31°E/30–41°N) above the EM. This subsidence index is closely connected to the ascending air and precipitation over the Bay of Bengal (Tyrlis et al., 2013; Rizou et al., 2018). The time series was normalized such that positive index values represent weak monsoon and negative index values represent strong monsoon. We chose the 30 years with the highest index (the weakest monsoon years) and averaged the Mediterranean's SST of those years. The same was done with the 30 years with the lowest index (strongest monsoon years). The difference between highest-index years and lowest-index years clearly shows that the effect of the subsidence over the EM is similar in both periods and in both models (Fig. 7). The results support the claim that the Etasian winds cooling effect is more dominant than the adiabatic heating by descending air (Poupkou et al., 2011; Tyrlis et al., 2013; Harpaz et al., 2014). The SST in the EM is much warmer in years of weak monsoon (high index value) than in years with strong monsoon (low index value). This is better expressed in the MPI-ESM-P model but is also well evident in the CCSM4 model. The similarity in Mediterranean's summer SST response to SAM strength in the MCA versus the LIA indicates that the southeastern variability source is minor in those periods. We also examined the difference in pressure tendency maps between the MCA and LIA (Fig. 8) and found differences of an order of magnitude lower than the differences between pre-IP and IP periods (Fig. 4), indicating the SAM did not change much between the MCA and the LIA.

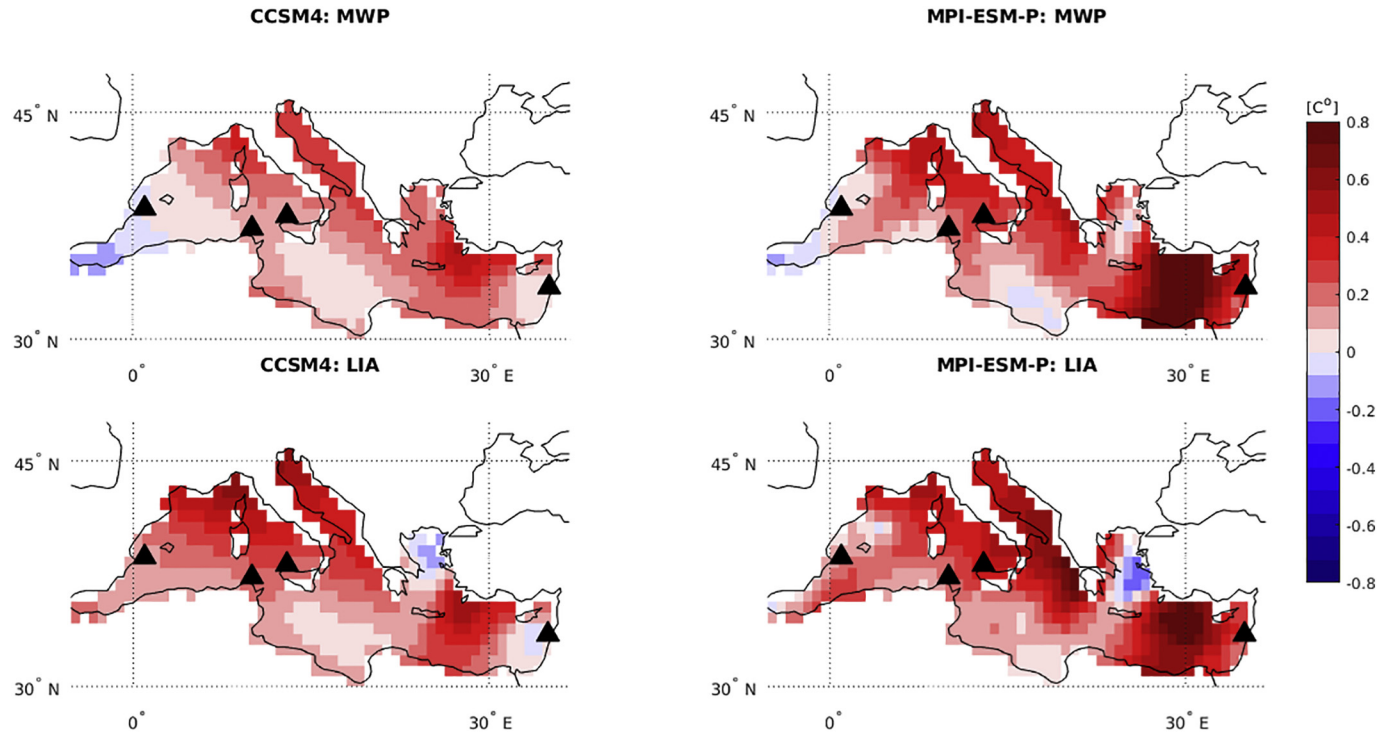

Fig. 7. Mediterranean SST difference from the CMIP5/PMIP3 models between years with high subsidence related to strong monsoon minus years with weak subsidence related to weak monsoon during MCA (900–1200 CE; upper row) and during LIA (1400–1700 CE; lower row). Vermetid rough locations are in black triangles.

3.2. Model simulations compared with vermetids 13C records

The connection between climatic systems and the carbon isotopic composition of vermetids, which represents the surface $\delta^{13}C$ of DIC (Sisma-Ventura et al., 2009), is more complex than their connection with oxygen isotopic composition. This complexity reflects the biological productivity in the upper level of the water column and the changes in atmospheric CO_2 isotopic composition due to enhanced fossil fuel combustion (the Suess effect; e.g. Swart et al., 2010). Photosynthesis preferentially removes ^{12}C, causing ^{13}C enrichment in the DIC pool. Hence, it is expected that a weak water column stratification will coincide with heavy $\delta^{13}C$ values of the DIC and vice versa. However, the general depletion trend observed during the IP, which is the prominent signal in the vermetid records, is mainly due to the Suess effect and a general increase in oligotrophy of the EM (Sisma-Ventura et al., 2014).

The $\delta^{13}C$ values in the EM, Tunis, and Spain composite records are similar in the period 900–1700 CE (Fig. 2), and although the Sicilian composite record is shifted by about 0.5, this suggests a background factor that is common to both the WM and EM. Indeed, the Atlantic Ocean is the main contributor of nutrients to the Mediterranean surface water (Myers et al., 1998; Krom et al., 2010; Powley et al., 2017) and controls primary production. The short residence time in the Mediterranean (less than 100 y; Roether and Schlitzer, 1991) plays a major role in making the WM and EM DIC isotopic composition uniform on a low-frequency time scale. All records also show the initiation of the Suess effect depletion around year 1850 CE, indicating an efficient atmospheric–ocean equilibrium. This may add to the similarity in background $\delta^{13}C$ values before the IP. The heavier isotopic composition of $\delta^{13}C$ of the Sicilian record during the years 850–1600 CE might be attributed to the Sicily Strait bathymetric complexity or to the bidirectional flow in the strait or to atmospheric regimes. Myers et al. (1998) suggested that shoaling of the pycnocline, resulting from strait features, indicates enhanced productivity during the Holocene due to enhanced vertical mixing. Others (Incarbona et al., 2008, 2016; Margaritelli et al., 2016) identified picks of high productivity in the Tyrrhenian basin surface water around 1000 CE, 1200 CE and 1600 CE in relation to increased heat flux or intensification of northwesterly winds associated with Atmospheric Blocking events (Moffa-Sánchez et al., 2014). Our vermetid based record resolution can not resolve these reported picks.

A time series of the vermetid $\delta^{13}C$ anomalies is plotted against upper water layer stratification anomalies (Fig. 9). The stratification strength is prescribed by the difference between potential densities at 100 m depth minus 10 m depth in order to study the high frequency variation in DIC isotopic composition. Low and high density differences stand for weak and strong water column stratification, respectively. Each region has different pre-IP $\delta^{13}C$ temporal features: The EM exhibits centennial variability in the $\delta^{13}C$ record, suggesting large fluctuations in the productivity of the EM surface layer (Sisma-Ventura et al., 2014) that was also observed by Schilman et al. (2001) in the high productivity period between 1350 and 1470. The stratification of the EM in both models also shows centennial variability but not entirely coherent with the $\delta^{13}C$ phase. For the vermetid cores from Spain the $\delta^{13}C$ of DIC does not show any significant trend from the beginning of the millennium until the rise during the IP. In Sicily there is a consistent decreasing trend in $\delta^{13}C$ of DIC in the years 850–1750 CE (of $\sim$ 0.5) that is not seen by a stratification trend in the models. The Tunis record shows lower $\delta^{13}C$ values in the years 1300–1600 CE that are in agreement with an enhanced stratification according to the models. Overall, stratification partly explains trends that are seen in the $\delta^{13}C$ records before the IP.

The spatial variability in $\delta^{13}C$ within the Mediterranean Sea, indicated by the different trends in the different records, was also noted by Salgado-Hernanz et al. (2019), who observed large regional variations in phytoplankton chlorophyll over the period of 1998–2014. They suggested that the response of phytoplankton to climate forcing is regionally driven. However, there is a feature that is common to all locations. Around the beginning of the IP (1800 CE), the $\delta^{13}C$ of DIC decreases while the stratification becomes stronger (as a consequence of surface warming). The trend in the $\delta^{13}C$ is more robust than the trend in stratification due to its strong association with the atmospheric Suess

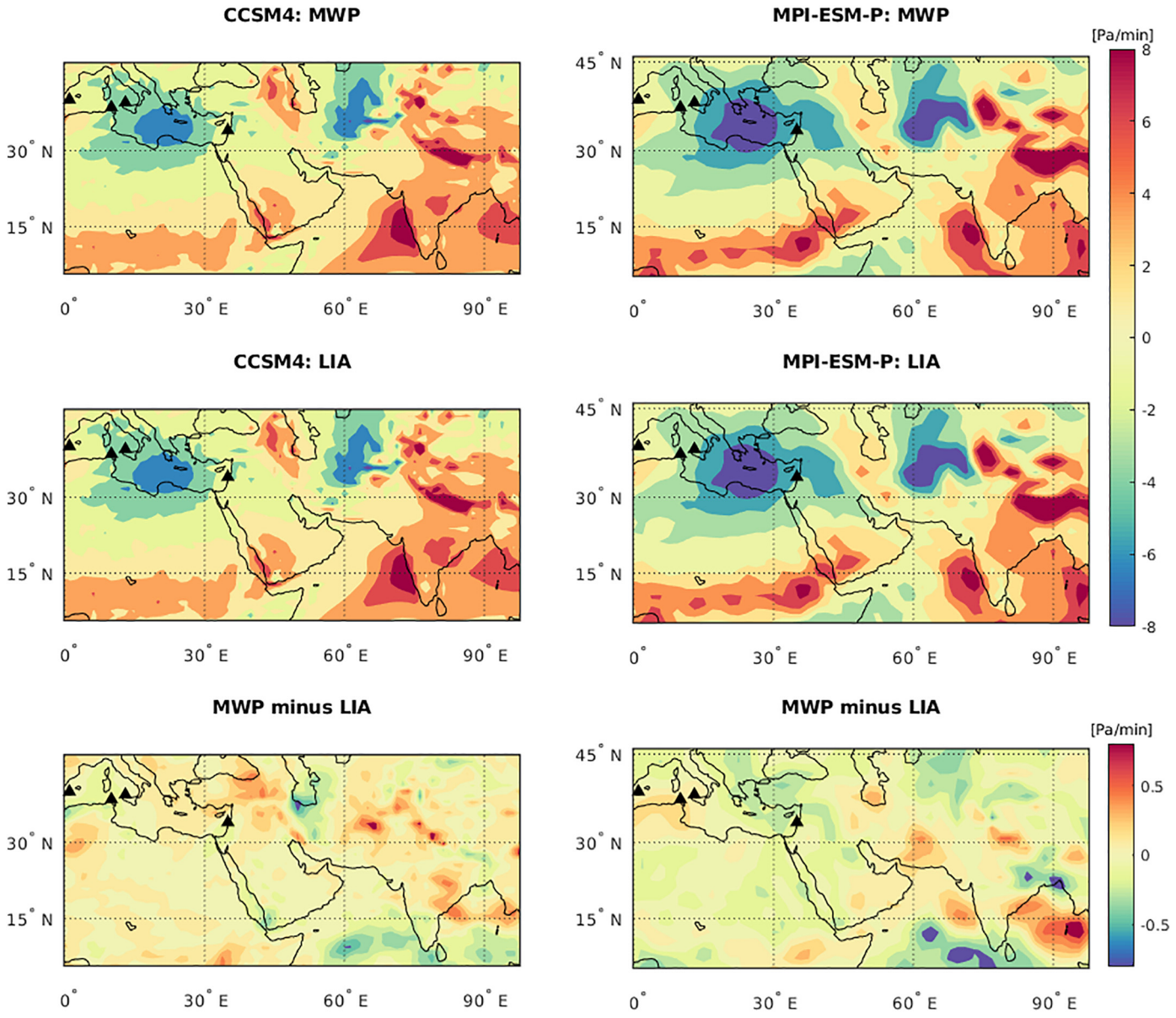

Fig. 8. Pressure tendency from the CMIP5/PMIP3 models in July at 500 hPa over the South Asian Monsoon and the Eastern Mediterranean area in the MCA (900–1200 CE), the LIA (1400–1700 CE) and the difference between them. In the two upper rows, blue (red) colors denote subsidence (ascent).

effect (Sisma-Ventura et al., 2014). An overall decline in productivity is revealed from the vermetid $\delta^{13}C$ from the beginning of the millennium until 2000 CE (Tunisian record has an exceptional low-frequency depletion in the middle of the millennium). Therefore, we calculated the zonal overturning circulation during the last millennium, the IP, and the difference between them (Fig. 10). The zonal overturning circulation is a meridional integration of the zonal velocity which is integrated from the bottom upward and is used to identify changes in the thermohaline circulation (Somot et al., 2006; Adloff et al., 2015). Both models seem to suggest that the surface Atlantic inflow (represented by the red filled contours, which is a clockwise circulation cell, at the surface) was stronger in the pre-IP millennial period than it is during the IP. Hence, the influx of nutrients to the surface water was more rapid and might explain some of the low productivity signals (depletion) in the recent period (1900–2000 CE) compared to the rest of the millennium. The sub-surface, counterclockwise cell (blue filled contours), also shows an enhanced pre-IP circulation in both models that is probably reacting to the enhanced surface circulation but is too deep to affect surface productivity.

4. Summary and conclusions

Vermetid cores collected from four different locations along the Mediterranean Sea were analyzed for $\delta^{18}O$ and $\delta^{13}C$, and the results were compared to simulated physical parameters in the broad frame of Earth System models. These organisms live in the intertidal zone and their aragonite skeleton can potentially record the variability of both atmospheric and oceanic parameters. Hence both atmospheric and oceanic parameters were tested and analyzed using the CMIP5/PMIP3 models, according to the mode of climatic variability that can explain the low and high frequency trends. Time series of oxygen and carbon isotopic composition of vermetid skeletons obtained from the west and east Mediterranean reefs reveal that the different parts of the sea surface have different thermal and productive behaviors throughout the last millennium.

Our results show that the EM SST has been increasing more rapidly than the WM SST since ~ 1800 CE, consistent with recent observations (Skliris et al., 2012; Macias et al., 2013). We examined the changes in the South Asian Monsoon influence on the EM SST to find that its

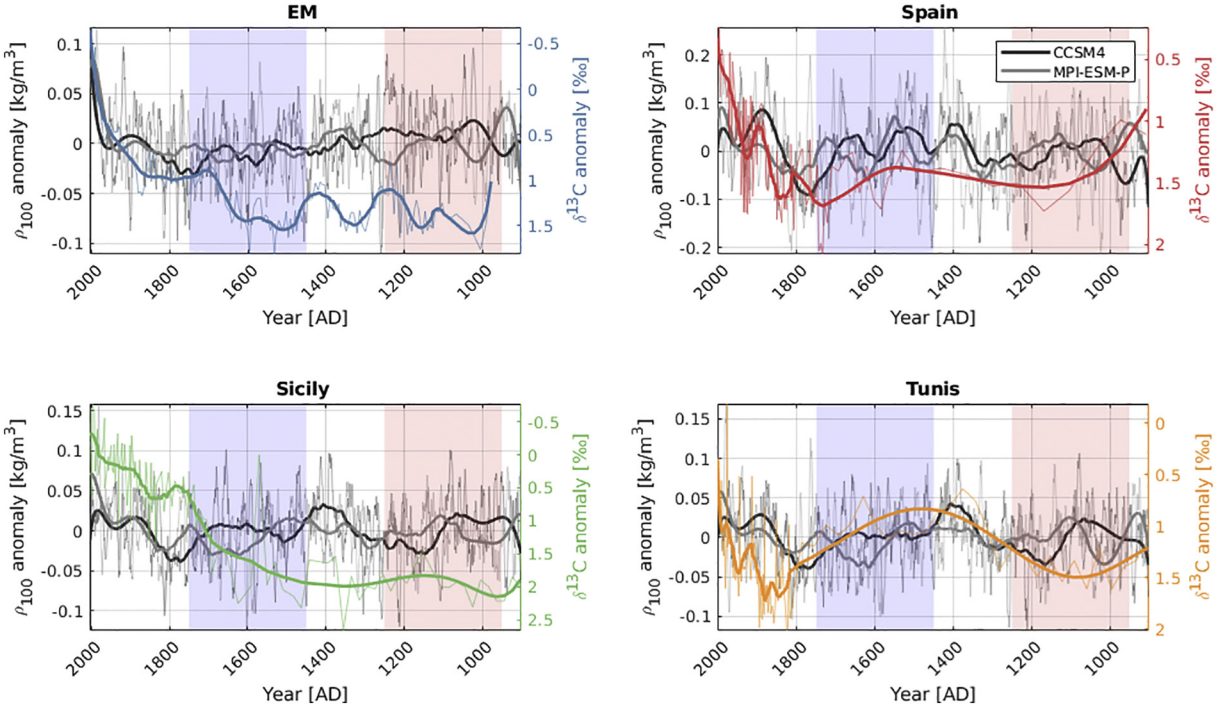

Fig. 9. Vertical density gradient ($\rho_{100} - \rho_{10}$) anomalies time series of four CMIP5/PMIP3 models compared with the $\delta^{13}C$ anomalies time series from the vermetid in each location. Shaded areas stand for the Medieval Climate Anomaly (MCA, red 900–1200 CE) and the Little Ice Age (LIA, blue 1400–1700 CE).

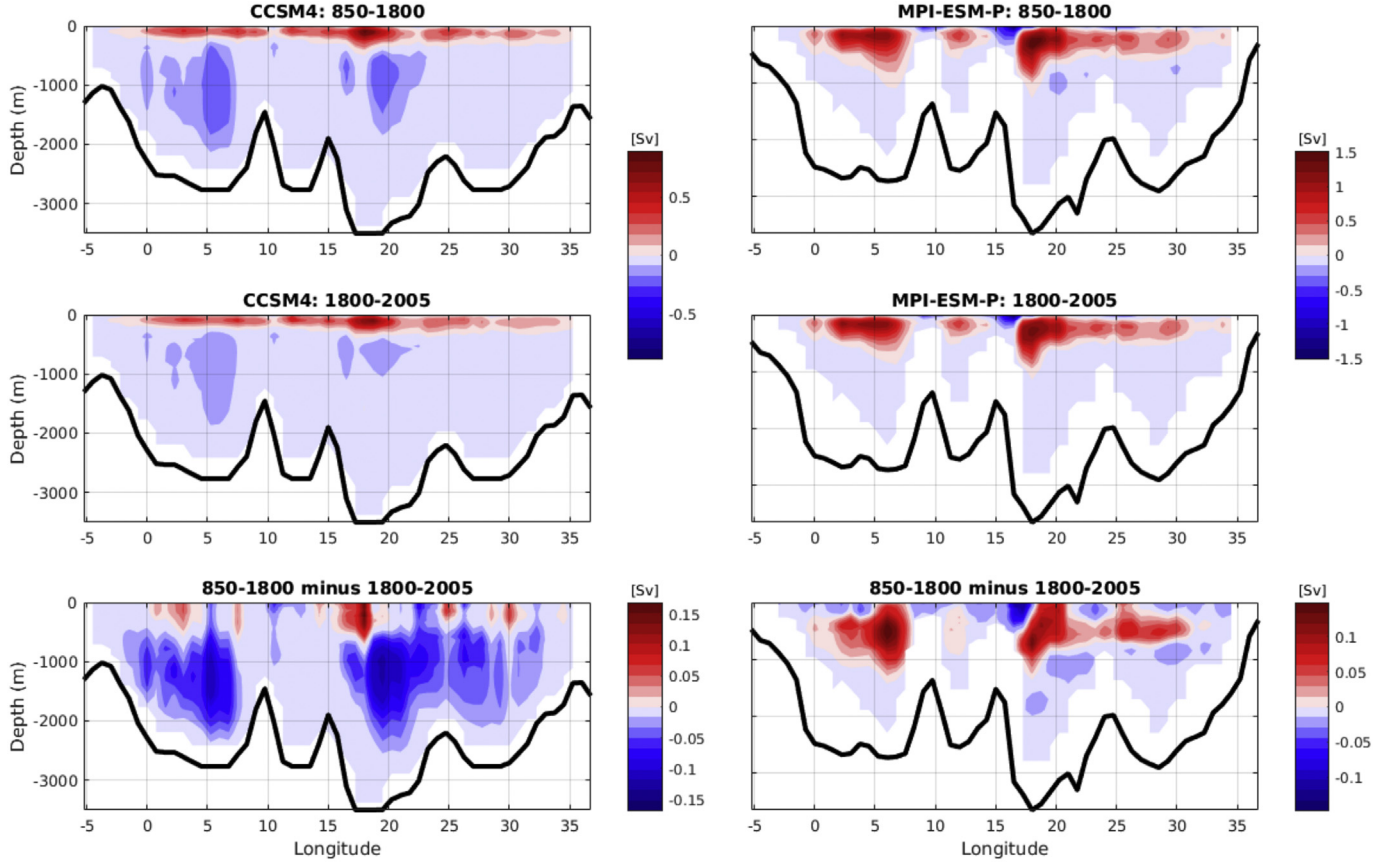

Fig. 10. Zonal overturning circulation of the Mediterranean from the CMIP5/PMIP3 models averaged over the last millennium (850–1800), the Industrial Period (1800–2005) and the difference between them.

influence has weakened during the last ~250 years. This weakening caused a decreased cooling by the Etasian winds enabling a more rapid warming of the EM under recent global warming. Furthermore, our analysis of the Mediterranean SST response to the SAM index shows that the dominant factor influencing the EM are the Etasian winds (cooling under strong Monsoon) and not the larger-scale subsidence (warming under strong Monsoon).

Another prominent result shown by our analysis is that during the MCA the NAO centers were more northern than their location during the LIA. This important result was drawn from examining the NAO pattern (i.e., regressed surface pressure) difference between the MCA and the LIA. Under the present climate, according to the models, the centers lay in between those two states, but closer to an MCA state. The Mediterranean's summer SST maps show that during the LIA, the EM and WM response to the NAO was likewise (warming under positive NAO index) and during the MCA it was opposite (WM warming and EM cooling under positive NAO index). This can result from the location of the sub-tropical jet, a dominant component of the NAO system, effecting the weather across Europe and its periphery.

The very similar $\delta^{13}C$, isotopic composition recorded by the vermetids along the Mediterranean Sea, which is mostly apparent in the years before the IP, indicate a uniform Atlantic inflow background effect. In all records the depletion due to the Suess effect started simultaneously, implying a strong coupling of the atmosphere-ocean systems in the Mediterranean. The high frequency variation seen in the EM is attributed to regional effects, such as the Nile inflow (Schilman et al., 2001; Hennekam et al., 2014). However, this is still debated, as Sisma-Ventura et al. (2014) showed a low correlation between the record of the Nile floods maxima and the EM $\delta^{13}C$ DIC vermetid-based record. Therefore, other sources of variability should be examined in relation to this high resolution record of DIC in the EM in the future.

Supplementary data to this article can be found online at https://doi.org/10.1016/j.gloplacha.2020.103159.

Acknowledgements

We are thankful to S.J. Fallon for the extensive dating analysis of the vermetid samples following his collaboration with the late Prof. S. Silenzi and to Y. Jacobson for his help in sample preparation for NOSAMS ^{14}C dating. We also thank I. Brailovsky for technical support. This study was supported by the de Botton center for Marine Research of the Weizmann Institute and by the Israel Science Foundation grant 1246/12 to A.S. Support provided to Y. Amitai by the Mediterranean Sea Research Center of Israel. This is CNR-ISMAR scientific contribution n. 2005.

References

Abish, B., Joseph, P.V., Johannessen, O.M., 2013. Weakening trend of the tropical easterly jet stream of the boreal summer monsoon season 1950-2009. J. Clim. 26 (23), 9408–9414.

Adloff, F., Somot, S., Sevault, F., Jordà, G., Aznar, R., Déqué, M., Herrmann, M., Marcos, M., Dubois, C., Padorno, E., Alvarez-Fanjul, E., Gomis, D., 2015. Mediterranean Sea response to climate change in an ensemble of twenty first century scenarios. Clim. Dyn. 45 (9–10), 2775–2802.

Anderson, D.M., Overpeck, J.T., Gupta, A.K., 2002. Increase in the asian southwest monsoon during the past four centuries. Science 297 (5581), 596–599.

Antonioli, F., 2002. New data on the Holocenic Sea-level rise in NW Sicily (Central Mediterranean Sea). Glob. Planet. Chang. 34 (1–2), 121–140.

Antonioli, F., Chemello, R., Improta, S., Riggio, S., 1999. *Dendropoma* lower intertidal reef formations and their palaeoclimatological significance, NW Sicily. Mar. Geol. 161 (2–4), 155–170.

Ausín, B., Flores, J.A., Sierro, F.J., Cacho, I., Hernández-Almeida, I., Martrat, B., Grimalt, J.O., 2015. Atmospheric patterns driving Holocene productivity in the Alboran Sea (Western Mediterranean): a multiproxy approach. The Holocene 25 (4), 583–595.

Berman, T., Azov, Y., Schneller, A., Walline, P., Townsend, D., 1986. Extent, transparency, and phytoplankton distribution of the neritic waters overlying the israeli coastal shelf. Oceanol. Acta Paris 9 (4), 439–447.

Böhm, F., Joachimski, M.M., Dullo, W.C., Eisenhauer, A., Lehnert, H., Reitner, J., Wörheide, G., 2000. Oxygen isotope fractionation in marine aragonite of coralline sponges. Geochim. Cosmochim. Acta 64 (10), 1695–1703.

Bonomo, S., Cascella, A., Alberico, I., Sorgato, S., Pelosi, N., Ferraro, L., Lirer, F., Vallefuoco, M., Bellucci, L., Agnini, C., et al., 2016. Reworked Coccoliths as runoff proxy for the last 400 years: the case of Gaeta Gulf (Central Tyrrhenian Sea, Central Italy). Palaeogeogr. Palaeoclimatol. Palaeoecol. 459, 15–28.

Calvo, M., Templado, J., Oliverio, M., Machordom, A., 2009. Hidden mediterranean biodiversity: molecular evidence for a cryptic species complex within the reef building vermetid gastropod dendropoma petraeum (mollusca: Caenogastropoda). Biol. J. Linn. Soc. 96 (4), 898–912.

Cisneros, M., Cacho, I., Frigola, J., Canals, M., Martrat, B., Casado, M., Grimalt, J., Pena, L., Margaritelli, G., Lirer, F., et al., 2016. Sea surface temperature variability in the Central-Western Mediterranean Sea during the last 2700 years: a multi-proxy and multi-record approach. Clim. Past 12 (4).

Fallon, S., Fifield, L.K., Chappell, J., 2010. The next chapter in radiocarbon dating at the Australian National University: status report on the single stage AMS. Nucl. Instrum. Methods Phys. Res., Sect. B 268 (7–8), 898–901.

Gogou, A., Triantaphyllou, M., Xoplaki, E., Izdebski, A., Parinos, C., Dimiza, M., Bouloubassi, I., Luterbacher, J., Kouli, K., Martrat, B., et al., 2016. Climate variability and socio-environmental changes in the northern Aegean (NE Mediterranean) during the last 1500 years. Quat. Sci. Rev. 136, 209–228.

Goudeau, M.-L.S., Reichart, G.-J., Wit, J., de Nooijer, L., Grauel, A.-L., Bernasconi, S., de Lange, G., 2015. Seasonality variations in the Central Mediterranean during climate change events in the late Holocene. Palaeogeogr. Palaeoclimatol. Palaeoecol. 418, 304–318.

Grauel, A.-L., Leider, A., Goudeau, M.-L.S., Müller, I.A., Bernasconi, S.M., Hinrichs, K.-U., de Lange, G.J., Zonneveld, K.A., Versteegh, G.J., 2013. What do SST proxies really tell us? A high-resolution multiproxy (UK37, TEXH86 and foraminifera δ18O) study in the Gulf of Taranto, Central Mediterranean Sea. Quat. Sci. Rev. 73, 115–131.

Harpaz, T., Ziv, B., Saaroni, H., Beja, E., 2014. Extreme summer temperatures in the East Mediterranean-dynamical analysis. Int. J. Climatol. 34 (3), 849–862.

Hennekam, R., Jilbert, T., Schnetger, B., de Lange, G.J., 2014. Solar forcing of Nile discharge and sapropel S1 formation in the early to middle Holocene eastern Mediterranean. Paleoceanography 29 (5), 343–356.

Herut, B., Krom, M.D., Pan, G., Mortimer, R., 1999. Atmospheric input of nitrogen and phosphorus to the Southeast Mediterranean: sources, fluxes, and possible impact. Limnol. Oceanogr. 44 (7), 1683–1692.

Hurrell, J.W., 1995. Decadal trends in the North Atlantic Oscillation: regional temperatures and precipitation. Science 269 (5224), 676–679.

Incarbona, A., Di Stefano, E., Patti, B., Pelosi, N., Bonomo, S., Mazzola, S., Sprovieri, R., Tranchida, G., Zgozi, S., Bonanno, A., 2008. Holocene millennial-scale productivity variations in the Sicily Channel (Mediterranean Sea). Paleoceanography 23 (3).

Incarbona, A., Martrat, B., Mortyn, P.G., Sprovieri, M., Ziveri, P., Gogou, A., Jordà, G., Xoplaki, E., Luterbacher, J., Langone, L., et al., 2016. Mediterranean circulation perturbations over the last five centuries: Relevance to past Eastern Mediterranean Transient-type events. Sci. Rep. 6, 29623.

Jacobson, Y., 2018. Reconstruction of Trace Element Variability in the Reef Builder Vermetid *Dendropoma petraeum* From the Mediterranean Sea During the Last Millennium. Ph.D. thesis. Weizmann Institute of Science.

Jalali, B., Sicre, M.-A., Klein, V., Schmidt, S., Maselli, V., Lirer, F., Bassetti, M.-A., Toucanne, S., Jorry, S.J., Insinga, D.D., Petrosino, P., Châles, F., 2018. Deltaic and coastal sediments as recorders of Mediterranean regional climate and human impact over the past three millennia. Paleoceanogr. Paleoclimatol. 33 (6), 579–593.

Jones, P., Jonsson, T., Wheeler, D., 1997. Extension to the North Atlantic Oscillation using early instrumental pressure observations from Gibraltar and south-West Iceland. Int. J. Climatol. 17 (13), 1433–1450.

Jones, P.D., Osborn, T.J., Briffa, K.R., 2003. Pressure-based measures of the North Atlantic Oscillation (NAO): A comparison and an assessment of changes in the strength of the NAO and in its influence on surface climate parameters. In: Geophysical Monograph Series. 134. Wiley Online Library, pp. 51–62.

Josey, S.A., Somot, S., Tsimplis, M., 2011. Impacts of atmospheric modes of variability on Mediterranean Sea surface heat exchange. J. Geophys. Res. 116 (C2), C02032.

Katrantsiotis, C., Norström, E., Smittenberg, R.H., Finne, M., Weiberg, E., Hättestrand, M., Avramidis, P., Wastegård, S., 2019. Climate changes in the Eastern Mediterranean over the last 5000 years and their links to the high-latitude atmospheric patterns and Asian monsoons. Glob. Planet. Chang. 175, 36–51.

Kondrashov, D., Feliks, Y., Ghil, M., 2005. Oscillatory modes of extended Nile River records (AD 622–1922). Geophys. Res. Lett. 32 (10).

Krishnan, R., Sabin, T.P., Vellore, R., Mujumdar, M., Sanjay, J., Goswami, B.N., Hourdin, F., Dufresne, J.-L., Terray, P., 2016. Deciphering the desiccation trend of the south Asian monsoon hydroclimate in a warming world. Clim. Dyn. 47 (3–4), 1007–1027.

Krom, M.D., Woodward, E.M., Herut, B., Kress, N., Carbo, P., Mantoura, R.F., Spyres, G., Thingsted, T.F., Wassmann, P., Wexels-Riser, C., Kitidis, V., Law, C., Zodiatis, G., 2005. Nutrient cycling in the south east Levantine basin of the eastern Mediterranean: results from a phosphorus starved system. Deep-Sea Res. II 52 (22 – 23), 2879–2896.

Krom, M.D., Emeis, K.C., Van Cappellen, P., 2010. Why is the Eastern Mediterranean phosphorus limited? Prog. Oceanogr. 85 (3–4), 236–244.

Krom, M., Kress, N., Berman-Frank, I., Rahav, E., 2014. Past, present and future patterns in the nutrient chemistry of the Eastern Mediterranean. In: Goffredo, S., Dubinsky, Z. (Eds.), The Mediterranean Sea. Springer, pp. 49–68.

Lohmann, G., 2008. Linking data and models. PAGES News 16 (2), 4–5.

Luterbacher, J., Xoplaki, E., 2003. 500-year winter temperature and precipitation variability over the Mediterranean area and its connection to the large-scale atmospheric circulation. In: Mediterranean Climate. Springer, pp. 133–153.

Luterbacher, J., Dietrich, D., Xoplaki, E., Grosjean, M., Wanner, H., 2004. European seasonal and annual temperature variability, trends, and extremes since 1500. Science 303 (5663), 1499–1503.

Luterbacher, J., García-Herrera, R., Akcer-On, S., Allan, R., Alvarez-Castro, M.C., Benito, G., Booth, J., Büntgen, U., Cagatay, N., Colombaroli, D., Davis, B., Esper, J., Felis, T., Fleitmann, D., Frank, D., Gallego, D., Garcia-Bustamante, E., Glaser, R., Gonzalez-Rouco, F.J., Goosse, H., Kiefer, T., Macklin, M.G., Manning, S.W., Montagna, P., Newman, L., Power, M.J., Rath, V., Ribera, P., Riemann, D., Roberts, N., Sicre, M.A., Silenzi, S., Tinner, W., Tzedakis, P.C., Valero-Garcés, B., van der Schrier, G., Vannière, B., Vogt, S., Wanner, H., Werner, J.P., Willett, G., Williams, M.H., Xoplaki, E., Zerefos, C.S., Zorita, E., 2012. A Review of 2000 Years of Paleoclimatic Evidence in the Mediterranean. Elsevier Inc.

Macias, D., Garcia-Gorriz, E., Stips, A., 2013. Understanding the causes of recent warming of Mediterranean waters. How much could be attributed to climate change? PLoS One 8 (11), e81591.

Mann, M.E., Jones, P.D., 2003. Global surface temperatures over the past two millennia. Geophys. Res. Lett. 30 (15), 15–18.

Mann, M.E., Zhang, Z., Rutherford, S., Bradley, R.S., Hughes, M.K., Shindell, D., Ammann, C., Faluvegi, G., Ni, F., 2009. Global signatures and dynamical origins of the Little Ice Age and medieval climate Anomaly. Science 326 (5957), 1256–1260.

Margaritelli, G., Vallefuoco, M., Di Rita, F., Capotondi, L., Bellucci, L., Insinga, D., Petrosino, P., Bonomo, S., Cacho, I., Cascella, A., et al., 2016. Marine response to climate changes during the last five millennia in the Central Mediterranean Sea. Glob. Planet. Chang. 142, 53–72.

Margaritelli, G., Cisneros, M., Cacho, I., Capotondi, L., Vallefuoco, M., Rettori, R., Lirer, F., 2018. Climatic variability over the last 3000years in the central - western Mediterranean Sea (Menorca Basin) detected by planktonic foraminifera and stable isotope records. Glob. Planet. Chang. 169 (March), 179–187.

Marullo, S., Artale, V., Santoleri, R., 2011. The SST multidecadal variability in the Atlantic-Mediterranean region and its relation to AMO. J. Clim. 24 (16), 4385–4401.

Metaxas, D., Bartzokas, A., Vitsas, A., 1991. Temperature-fluctuations in the Mediterranean area during the last 120 years. Int. J. Climatol. 11 (8), 897–908.

Moberg, A., Sonechkin, D.M., Holmgren, K., Datsenko, N.M., Karlén, W., 2005. Highly variable Northern Hemisphere temperatures reconstructed from low- and high-resolution proxy data. Nature 433 (7026), 613–617.

Moffa-Sánchez, P., Born, A., Hall, I.R., Thornalley, D.J., Barker, S., 2014. Solar forcing of North Atlantic surface temperature and salinity over the past millennium. Nat. Geosci. 7 (4), 275.

Montagna, P., Silenzi, S., Devoti, S., Mazzoli, C., McCulloch, M., Scicchitano, G., Taviani, M., 2008. Climate reconstructions and monitoring in the Mediterranean Sea: a review on some recently discovered high-resolution marine archives. Rendiconti Lincei 19 (2), 121–140.

Moreno, A., Pérez, A., Frigola, J., Nieto-Moreno, V., Rodrigo-Gámiz, M., Martrat, B., González-Sampériz, P., Morellón, M., Martín-Puertas, C., Corella, J.P., Belmonte, Á., Sancho, C., Cacho, I., Herrera, G., Canals, M., Grimalt, J.O., Jiménez-Espejo, F., Martínez-Ruiz, F., Vegas-Vilarrúbia, T., Valero-Garcés, B.L., 2012. The medieval climate Anomaly in the Iberian Peninsula reconstructed from marine and lake records. Quat. Sci. Rev. 43, 16–32.

Myers, P.G., Haines, K., Rohling, E.J., 1998. Modeling the paleocirculation of the Mediterranean: the last Glacial Maximum and the Holocene with emphasis on the formation of sapropel S 1. Paleoceanography 13 (6), 586–606.

Pierre, C., 1999. The oxygen and carbon isotope distribution in the Mediterranean water masses. Mar. Geol. 153 (1–4), 41–55.

Poupkou, A., Zanis, P., Nastos, P., Papanastasiou, D., Melas, D., Tourpali, K., Zerefos, C., 2011. Present climate trend analysis of the Etesian winds in the Aegean Sea. Theor. Appl. Climatol. 106 (3–4), 459–472.

Powley, H.R., Krom, M.D., Van Cappellen, P., 2017. Understanding the unique biogeochemistry of the Mediterranean Sea: insights from a coupled phosphorus and nitrogen model. Glob. Biogeochem. Cycles 31 (6), 1010–1031.

Pozo-Vázquez, D., Esteban-Parra, M.J., Rodrigo, F.S., Castro-Díez, Y., 2001. A study of NAO variability and its possible non-linear influences on European surface temperature. Clim. Dyn. 17 (9), 701–715.

Rao, B.R., Rao, D.V., Rao, V.B., 2004. Decreasing trend in the strength of Tropical Easterly Jet during the Asian summer monsoon season and the number of tropical cyclonic systems over Bay of Bengal. Geophys. Res. Lett. 31 (14), 4–6.

Rizou, D., Flocas, H.A., Hatzaki, M., Bartzokas, A., 2018. A statistical investigation of the impact of the Indian monsoon on the Eastern Mediterranean circulation. Atmosphere 9 (3), 1–27.

Roberts, N., Moreno, A., Valero-Garcés, B.L., Corella, J.P., Jones, M., Allcock, S., Woodbridge, J., Morellón, M., Luterbacher, J., Xoplaki, E., TürkeÅŸ, M., 2012. Palaeolimnological evidence for an eastwest climate see-saw in the Mediterranean since AD 900. Glob. Planet. Chang. 84–85, 23–34.

Rodwell, M.J., Hoskins, B.J., 1996. Monsoons and the dynamics of deserts. Q. J. R. Meteorol. Soc. 122 (534), 1385–1404.

Roether, W., Schlitzer, R., 1991. Eastern Mediterranean deep water renewal on the basis of chlorofluoromethane and tritium data. Dyn. Atmos. Oceans 15 (3–5), 333–354.

Saenger, C., Came, R.E., Oppo, D.W., Keigwin, L.D., Cohen, A.L., 2011. Regional climate variability in the western subtropical North Atlantic during the past two millennia. Paleoceanography 26 (2), PA2206.

Safriel, U., 1975. The role of vermetid gastropods in the formation of Mediterranean and Atlantic reefs. Oecologia 20 (1), 85–101.

Salgado-Hernanz, P.M., Racault, M.F., Font-Muñoz, J.S., Basterretxea, G., 2019. Trends in phytoplankton phenology in the Mediterranean Sea based on ocean-colour remote sensing. Remote Sens. Environ. 221, 50–64.

Sandroni, V., Raimbault, P., Migon, C., Garcia, N., Gouze, E., 2007. Dry atmospheric deposition and diazotrophy as sources of new nitrogen to northwestern mediterranean oligotrophic surface waters. Deep-Sea Res. I Oceanogr. Res. Pap. 54 (11), 1859–1870.

Sathiyamoorthy, V., 2005. Large scale reduction in the size of the Tropical Easterly Jet. Geophys. Res. Lett. 32 (14), 1–4.

Schilman, B., Bar-Matthews, M., Almogi-Labin, A., Luz, B., 2001. Global climate instability reflected by Eastern Mediterranean marine records during the late Holocene. Palaeogeogr. Palaeoclimatol. Palaeoecol. 176 (1–4), 157–176.

Schmidt, G.A., Jungclaus, J.H., Ammann, C.M., Bard, E., Braconnot, P., Crowley, T.J., Delaygue, G., Joos, F., Krivova, N.A., Muscheler, R., Otto-Bliesner, B.L., Pongratz, J., Shindell, D.T., Solanki, S.K., Steinhilber, F., Vieira, L.E.A., 2012. Climate forcing reconstructions for use in PMIP simulations of the last Millennium (v1.1). Geosci. Model Dev. 5, 185–191.

Sicre, M.-A., Jalali, B., Martrat, B., Schmidt, S., Bassetti, M.-A., Kallel, N., 2016. Sea surface temperature variability in the North Western Mediterranean Sea (Gulf of Lion) during the Common Era. Earth Planet. Sci. Lett. 456, 124–133.

Silenzi, S., Antonioli, F., Chemello, R., 2004. A new marker for sea surface temperature trend during the last centuries in temperate areas: Vermetid reef. Glob. Planet. Chang. 40 (1–2), 105–114.

Sisma-Ventura, G., Guzner, B., Yam, R., Fine, M., Shemesh, A., 2009. The reef builder gastropod *Dendropoma petreaum* - a proxy of short and long term climatic events in the Eastern Mediterranean. Geochim. Cosmochim. Acta 73 (15), 4376–4383.

Sisma-Ventura, G., Yam, R., Shemesh, A., 2014. Recent unprecedented warming and oligotrophy of the eastern Mediterranean Sea within the last millennium. Geophys. Res. Lett. 41 (14), 5158–5166.

Skliris, N., Sofianos, S., Gkanasos, A., Mantziafou, A., Vervatis, V., Axaopoulos, P., Lascaratos, A., 2012. Decadal scale variability of sea surface temperature in the Mediterranean Sea in relation to atmospheric variability. Ocean Dyn. 62 (1), 13–30.

Somot, S., Sevault, F., Déqué, M., 2006. Transient climate change scenario simulation of the Mediterranean Sea for the twenty-first century using a high-resolution ocean circulation model. Clim. Dyn. 27 (7–8), 851–879.

Stuiver, M., Reimer, P., Reimer, R., 2017. CALIB 7.1 [WWW Program]. http://calib.org (Last accessed, 8–24).

Swart, P.K., Greer, L., Rosenheim, B.E., Moses, C.S., Waite, A.J., Winter, A., Dodge, R.E., Helmle, K., 2010. The 13C Suess effect in scleractinian corals mirror changes in the anthropogenic CO2 inventory of the surface oceans. Geophys. Res. Lett. 37 (5), L05604.

Trigo, R., Osborn, T., Corte-Real, J., 2002. The North Atlantic Oscillation influence on Europe: climate impacts and associated physical mechanisms. Clim. Res. 20, 9–17.

Trouet, V., Esper, J., Graham, N.E., Baker, A., Scourse, J.D., Frank, D.C., 2009. Persistent positive North Atlantic Oscillation mode dominated the medieval climate Anomaly. Science 324 (5923), 78–80.

Tyrlis, E., Lelieveld, J., Steil, B., 2013. The summer circulation over the Eastern Mediterranean and the Middle East: influence of the south Asian monsoon. Clim. Dyn. 40 (5–6), 1103–1123.

Ulbrich, U., Christoph, M., 1999. A shift of the NAO and increasing storm track activity over Europe due to anthropogenic greenhouse gas forcing. Clim. Dyn. 15 (7), 551–559.

Vargas-Yáñez, M., Jesús García, M., Salat, J., García-Martínez, M.C., Pascual, J., Moya, F., 2008. Warming trends and decadal variability in the Western Mediterranean shelf. Glob. Planet. Chang. 63 (2–3), 177–184.

Xoplaki, E., Luterbacher, J., González-Ruoco, F., 2006. Mediterranean summer temperature and winter precipitation, large-scale dynamics, trends. Nuovo cimento della Società Italiana di Fisica. B-Basic Top. Phys. 29 (1), 45–54.

Ziv, B., Saaroni, H., Alpert, P., 2004. The factors governing the summer regime of the eastern Mediterranean. Int. J. Climatol. 24 (14), 1859–1871.